ARTICLES
https://doi.org/10.1038/s41561-020-0583-4

nature geoscience



# Amplified transboundary transport of haze by aerosol–boundary layer interaction in China

Xin Huang[1,2], Aijun Ding[1,2]✉, Zilin Wang[1], Ke Ding[1], Jian Gao[3], Fahe Chai[3] and Congbin Fu[1,2]

**Although air quality in China has substantially improved since 2013 as a consequence of the clean air action, severe haze events still frequently strike megacities despite strict local emissions reduction efforts. Long-range transport and local accumulation as well as chemical transformation have been deemed as key factors of heavy haze pollution; however, the formation mechanisms of regional long-lasting haze and the physical and chemical connections between different megacities clusters are still poorly understood. Here we present that long-range transport and aerosol–boundary layer feedback may interact rather than act as two isolated processes as traditionally thought by investigating typical regional haze events in northern and eastern China. This interaction can then amplify transboundary air pollution transport over a distance of 1,000 km and boost long-lasting secondary haze from the North China Plain to the Yangtze River delta. Earlier emission reduction before the pollution episodes would provide better air pollution mitigation in both regions. Our results show an amplified transboundary transport of haze by aerosol–boundary layer interaction in China and suggest the importance of coordinated cross-regional emission reduction with a focus on radiatively active species like black carbon.**

Developed regions in China have been suffering from severe haze pollution in recent decades[1–3]. To tackle this great challenge, the Chinese government has implemented strict emission control measures in critical regions, such as the North China Plain (NCP) and the Yangtze River delta (YRD), since 2013[4–8]. Although the annual average concentration of fine particular matter ($PM_{2.5}$) has been substantially reduced[5,7], heavy haze pollution with $PM_{2.5}$ concentrations over 300 μg m$^{-3}$ still frequently engulfs megacities in both regions[2,9].

The causes of haze episodes in megacities have been intensively studied from different aspects. Transboundary long-range transport under specific weather conditions could trigger severe air pollution in some regions[3,4,9–11]. For example, a persistent weak southerly wind easily leads to severe air pollution in the NCP[3,12–14] while a cold front associated with strong wind could dissipate the locally accumulated pollutants in the NCP but conversely transport the pollution through a long distance to the YRD[11,15–17]. Locally, aqueous and heterogeneous reactions are the key processes that facilitate the fast formation of secondary particles[1,2,18–23], and aerosol–planetary boundary layer (PBL) interaction has recently been found to play crucial roles in the accumulation of locally emitted pollutants in megacities under stagnant weather and weakening monsoon[2,9,24–31]. However, because of complex transport scales and multiple species, understanding of the dominant process of haze formation in some regions is very difficult. For multiscale and multipollutant haze episodes between regions with a distance over 1,000 km (for example, the NCP and YRD), the main linkage between transboundary transport with aerosol–PBL interaction and secondary chemical production remains unclear.

By examining one of the typical cross-regional haze events in eastern China on the basis of comprehensive field measurements and model simulations, we demonstrate that transboundary transport of primary and secondary haze pollutants between the NCP and YRD can be amplified by aerosol–PBL interaction. Light-absorbing aerosols transported from the YRD to the upper PBL over the NCP cause strong aerosol–PBL interaction there and hence enhance the local pollution accumulation by stronger PBL stability and chemical production of secondary aerosols with elevated relative humidity. The enhanced haze pollution could be further transported back to the YRD by cold fronts. Our results show that a coordinated cross-regional reduction effort (for example, an emission reduction in the YRD two days before the predicted severe haze episode) could achieve more-efficient pollution mitigation in both regions than conventional emission control during haze events.

## Typical haze events with transboundary transport

In winter, haze pollution events in the NCP and YRD often occur alternately and most of the events in YRD are related to transboundary transport from the NCP by cold fronts[4,11,17]. The timeseries of $PM_{2.5}$ concentrations for 18 co-existing typical severe haze episodes in NCP and YRD cities in winter from 2013 to 2018 shows that a broader plume with higher peak concentration in the NCP was followed by a sharp and short one in the YRD (Fig. 1a and Supplementary Figs. 1 and 2). The outbreak of YRD pollution usually peaks with a time lag of 1–1.5 d after that in the NCP. During NCP haze events, observations from air-quality monitoring networks showed a quite high daily average $PM_{2.5}$ concentration (over 200 μg m$^{-3}$) and an overall northward circulation in coastal eastern China, under the influence of the weak anticyclone over the sea (Fig. 1b). Strong south-to-north gradients existed in the surface $PM_{2.5}$ concentrations between the YRD and NCP (Fig. 1b). However, during the YRD haze events in the following days, high $PM_{2.5}$ concentration plumes mainly concentrated over eastern China associated with strong outflow from the north (Fig. 1c), demonstrating a clear transboundary transport of regional-scale haze pollution.

A haze event around the end of 2017 provided a unique opportunity to conduct an intensive field campaign to identify the associated physical and chemical mechanisms. During this event, the

[1]Joint International Research Laboratory of Atmospheric and Earth System Sciences, School of Atmospheric Sciences, Nanjing University, Nanjing, China. [2]Collaborative Innovation Center of Climate Change, Jiangsu Province, Nanjing, China. [3]State Key Laboratory of Environmental Criteria and Risk Assessment, Chinese Research Academy of Environmental Sciences, Beijing, China. ✉e-mail: dingaj@nju.edu.cn

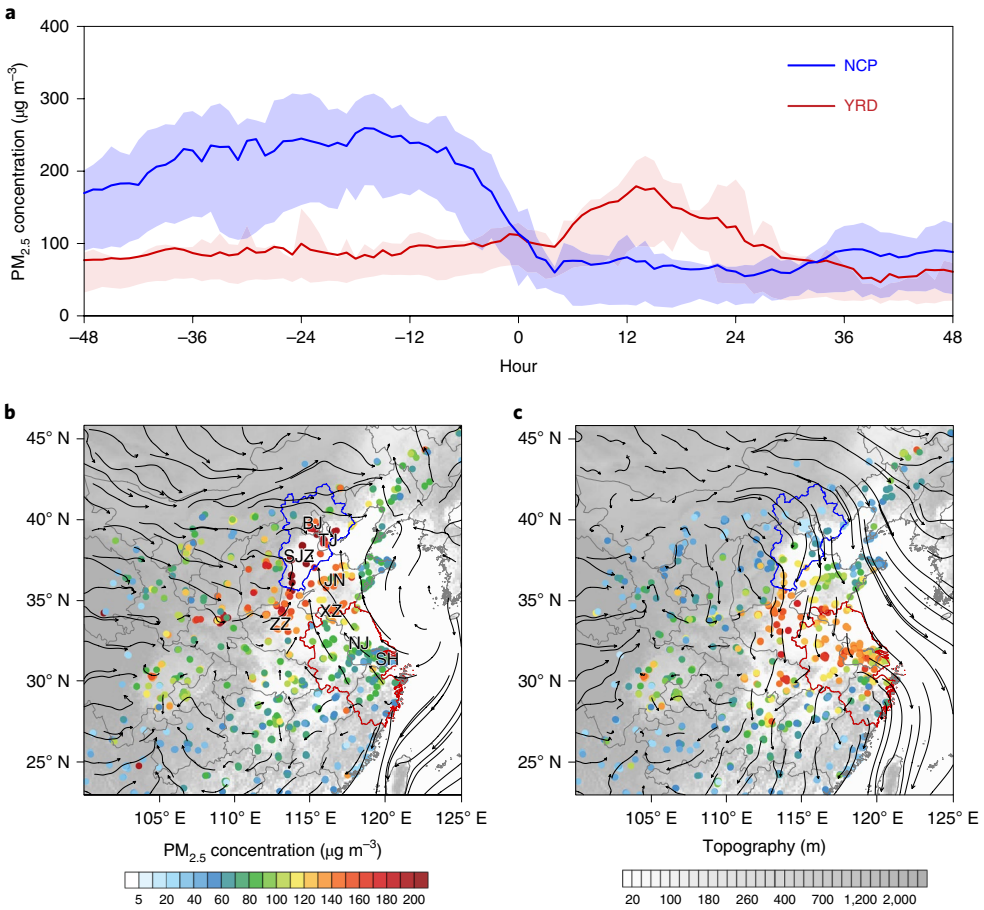


**Fig. 1 | Transboundary haze transport between northern and eastern China. a**, Average $PM_{2.5}$ concentrations in 18 typical co-existing haze events in the NCP and YRD during 2013–2018. Shaded areas mark the 25th–75th percentile range. **b**,**c**, Average of observed (dots) $PM_{2.5}$ concentrations and WRF-Chem simulated wind flows for the first and second half of these cross-regional haze events, respectively. Cities in the NCP (in blue) are Beijing (BJ), Tianjin (TJ) and Shijiazhuang (SJZ). YRD cities (in red) include Shanghai (SH), Nanjing (NJ) and Xuzhou (XZ). Zhengzhou (ZZ) and Jinan (JN) are between the two regions.

NCP was subjected to a long-lasting severe haze pollution with maximum $PM_{2.5}$ concentrations reaching 800 μg m$^{-3}$ in megacities such as Shijiazhuang on 29 December (Extended Data Fig. 1a). Over the next couple of days, cities from north to south (for example, Zhengzhou, Jinan, Xuzhou, Nanjing, Shanghai and so on) successively experienced multiple days of haze pollution with increasingly sharp peaks. On 31 December, the daily average of $PM_{2.5}$ concentration reached up to 273.5 μg m$^{-3}$ in Nanjing, which is the highest since 2015. It also featured the largest synoptic-scale variation over the past 5 yr according to ensemble empirical mode decomposition analysis (Extended Data Fig. 1b). This 1 d event increased the annual average of $PM_{2.5}$ concentration by over 1 μg m$^{-3}$ in Nanjing and Shanghai. Weather Research and Forecasting model coupled with Chemistry (WRF-Chem) simulations (Extended Data Fig. 1c,d) clearly showed that the transport pathways of this multiple-day event were similar to those averaged for the 18 typical episodes given in Fig. 1c,d. A recirculated transport pattern of air masses between cities in the YRD (for example, Nanjing) and NCP (Zhengzhou, Tianjin and Jinan) during 27–31 December 2017 was also identified by Lagrangian dispersion modelling (see Extended Data Fig. 2 and Methods).

## Impact of aerosol–PBL interaction on secondary haze

Previous studies have demonstrated that black carbon (BC), featuring strong radiative effect[32–36], plays an important role in aerosol–PBL interaction and subsequently intensifies near-surface haze pollution[2,9,28,37,38]. Considering this recirculated transport pattern, we examined the biases of air temperature and relative humidity (RH) between Global Forecast System (GFS) predictions and the radiosonde measurements (see Methods) along the transport pathway of the haze event. This comparison could help identify processes that have not been resolved in the weather forecast model, and aerosols have been proven to be one major contributor to such bias under polluted conditions[2,9]. As clearly demonstrated in Fig. 2a,b and Supplementary Fig. 3, the forecast bias increased substantially as pollution deteriorated along the transport pathways. The strong and increasing upper-PBL warming and lower-PBL dimming over the NCP together with a substantial enhancement in RH (20–50%) indicate an important role of aerosol–PBL interaction[2,9,24]. Figure 2c shows that observed $PM_{2.5}$ concentrations in Nanjing increased from 101 μg m$^{-3}$ on 26–27 December to 271 μg m$^{-3}$ on 30–31 December, together with a substantial increase in the sum of sulfate, nitrate and ammonium (SNA) fractions (from 44% to 57%). The observations along transport pathways also confirm an overall increase in the SNA/elemental carbon (EC) ratio during the episode (Fig. 2d). The WRF-Chem simulated SNA/BC (Fig. 2e) shows that only the simulation with aerosol–radiation interaction (ARI-on) can capture the increases (approximately 10–50%) in both primary and secondary PM levels along the transport pathway, compared with that without ARI (ARI-off). Here, the increase in the observed

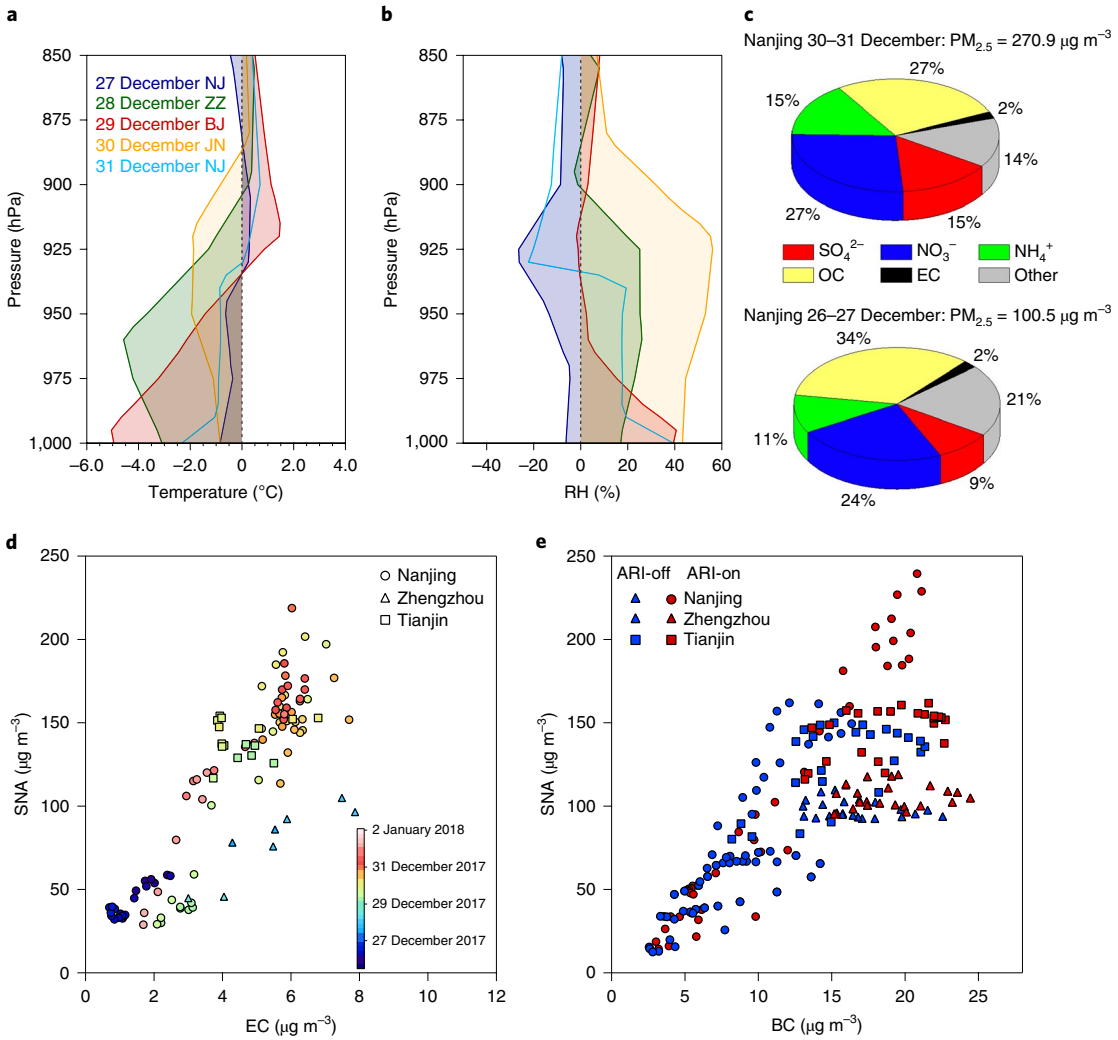


**Fig. 2 | Evolution of aerosol–PBL interaction and chemical compositions during the transboundary transport of haze. a**, Vertical distribution of air temperature difference between sounding observations and GFS 24 h forecasts for cities along the transport pathways of haze during 27–31 December 2017. **b**, Same as **a** except for RH. **c**, Observed $PM_{2.5}$ compositions in Nanjing for 26–27 and 30–31 December 2017, respectively. **d**, Scatter plot of observed SNA as a function of EC. **e**, Scatter plot of SNA as a function of BC derived from ARI-on/off runs of WRF-Chem.

EC and SNA concentrations is indicative of the respective effects of local pollution accumulation due to a more-stable PBL and secondary production induced by aerosol–PBL interaction.

Source apportionment based on WRF-Chem simulations suggests that the $PM_{2.5}$ concentration in the NCP has been substantially influenced by regional contributions from the YRD, Shandong province (SD) and other areas on 28 December, the day with rapid deterioration in haze pollution (Fig. 3a,b). Local (or subregional) contributions of NCP emissions declined with altitude, with the largest contributions from the YRD at an altitude of 700–800 m. In terms of BC, the absorbing aerosol with a strong 'dome effect', which means the upper atmospheric heating and surface dimming suppress PBL development and consequently enhance the occurrences of extreme haze pollution[2,9,26,28,37], the local contributions were much stronger in the lower PBL, while the regional contributions (especially those from the YRD) were quite substantial in the upper PBL. Comparatively, YRD contributions to secondary particles, such as sulfate and nitrate (SN), were more pronounced, reaching a contribution of nearly 50% at an altitude of approximately 700 m (Fig. 3a,b). Here, the distinct height dependence of regional contributions was mainly attributed to different transport pathways. In the upper PBL, rapid advection was capable of transporting more warm and humid air masses as well as aged BC, coated by secondary aerosols, with the strongest radiative heating[32–35] from the YRD region (Extended Data Figs. 3 and 4). Such a long-range transport from the YRD at an altitude of 700–800 m gave rise to a substantial aerosol–PBL interaction over the NCP because of a much stronger 'dome effect' of BC in the upper PBL compared with the locally emitted one near the surface[2,25] (Extended Data Fig. 5 and Supplementary Fig. 4).

The intense aerosol–PBL interaction in the NCP was not only characterized by a suppressed turbulent mixing associated with stable temperature stratification but also featured higher levels of humidity in the lower PBL (Fig. 2b). RH has been well acknowledged to be an important factor that influences the chemical formation of secondary aerosols through aqueous-phase and heterogeneous reactions[18,20–23,39]. The enhancement (positive bias) in RH was most pronounced in NCP cities (for example, Beijing and Shijiazhuang) on 29 December, exceeding 50% and accompanied by a negative bias of 5 K in air temperature (Fig. 2b). Vertical observations and simulations for Shijiazhuang show consistent results (Extended Data Fig. 4). The most obvious upper-air warming was observed on

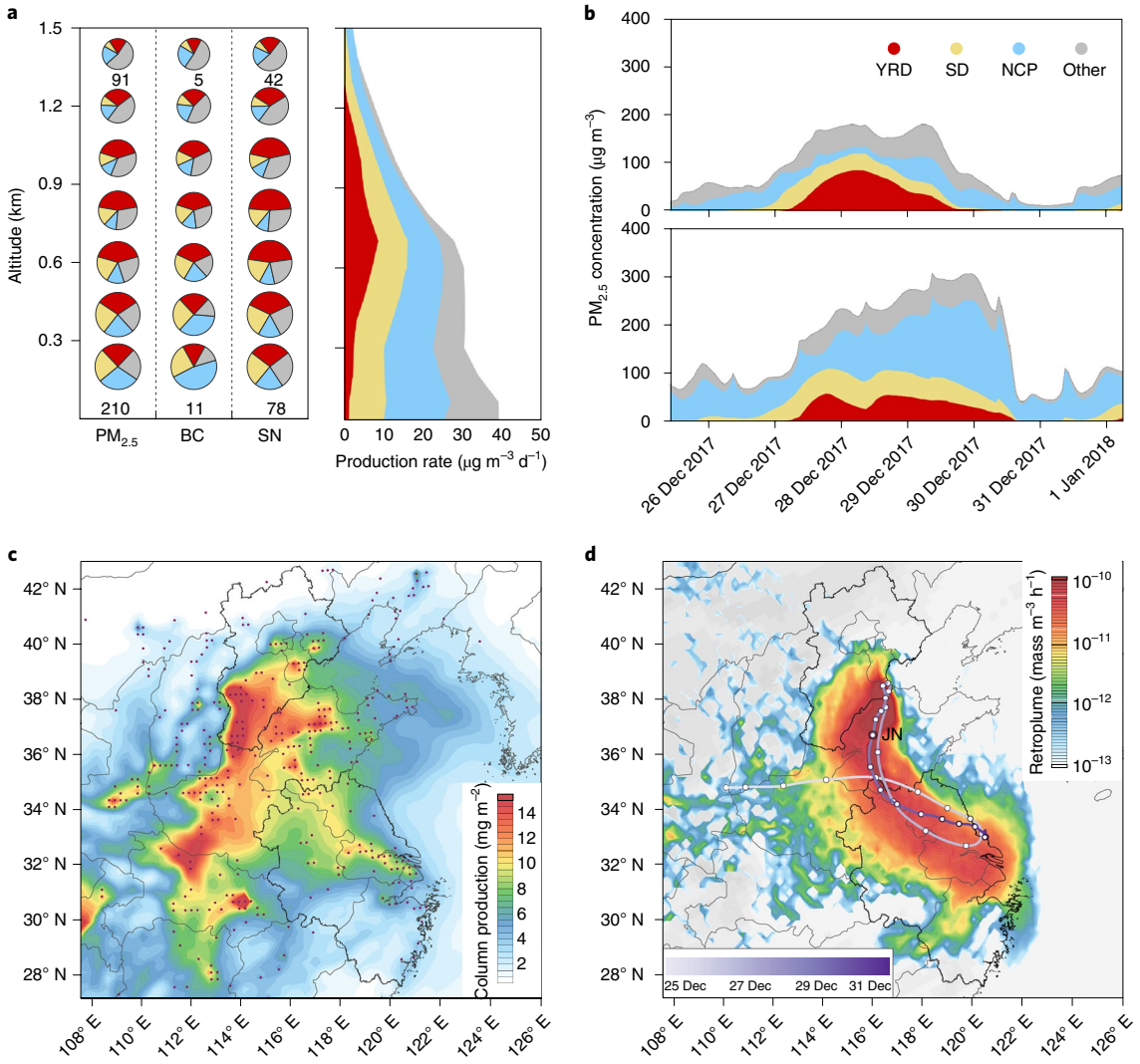


**Fig. 3 | Source appointment and transport pathway of haze. a**, Vertical distribution of WRF-Chem simulated $PM_{2.5}$, BC and SN source appointment and SN production rates for the NCP on 28 December 2017. The sizes of the pies denote concentrations with reference numbers in a unit of μg $m^{-3}$. **b**, WRF-Chem simulated $PM_{2.5}$ source appointment for 700 m altitude (upper panel) and the ground surface (lower panel) of the NCP. **c**, Average column production of sulfate during 27 December 2017 to 1 January 2018. **d**, Average retroplume and trajectories (in purple) for 5 d backward plus 3 d forward simulations for an altitude of 100 m over Jinan at 12:00 UTC on 29 December 2017.

28 December, corresponding to the strongest regional contributions from the YRD (Fig. 3a), while the following day (29 December) was characterized by the most remarkable dimming (−5 K) within an extremely shallow PBL (200–300 m). On that day, the largest gaps (over 300 μg $m^{-3}$) were found between observations and the ARI-off simulation of the peak $PM_{2.5}$ concentration, but the ARI-on simulation reasonably reproduced the extreme pollution levels (Extended Data Fig. 4b). As a consequence of concentrated precursors together with higher RH, the NCP became a breeding ground for secondary aerosols such as sulfate (Fig. 3c), even though $SO_2$ emissions were more intensive in Shandong and the YRD.

The regional source attribution of the YRD presents completely different characteristics from that of the NCP (Extended Data Fig. 6). Before 30 December, most $PM_{2.5}$ originated locally from the YRD when air masses were transported from the southeast. From 30 December 2017 to 1 January 2018, increases in $PM_{2.5}$ on the ground surface mainly originated from NCP, Shandong and other regions rather than from the YRD itself. Notably, as discussed in the preceding, NCP haze pollution was substantially enhanced by aerosol–PBL interaction two days before under the influence of regional transport from the south. Secondary particle production from regional and local precursors in the NCP was substantially enhanced by aerosol–PBL feedback and then played a vital role in increasing the peak concentration of $PM_{2.5}$ in the YRD associated with anticyclones and cold fronts.

## Conceptual scheme and implications for pollution control

On the basis of the preceding analysis, we propose a conceptual framework to demonstrate how aerosol–PBL interaction amplifies the transboundary transport of primary and secondary particles between the two regions (Fig. 4 and Extended Data Fig. 7). The key processes could be identified as three stages. At the first stage, air pollutants from the YRD can efficiently influence the PBL dynamics when they are transported to the upper PBL over the NCP, resulting in a suppressed PBL height and weakened turbulence, thereby facilitating local pollutant accumulation. During this stage, NCP haze is not necessarily related to the preceding heavy pollution in the YRD (Figs. 1a and 5a). During the second stage, the notable reduction in

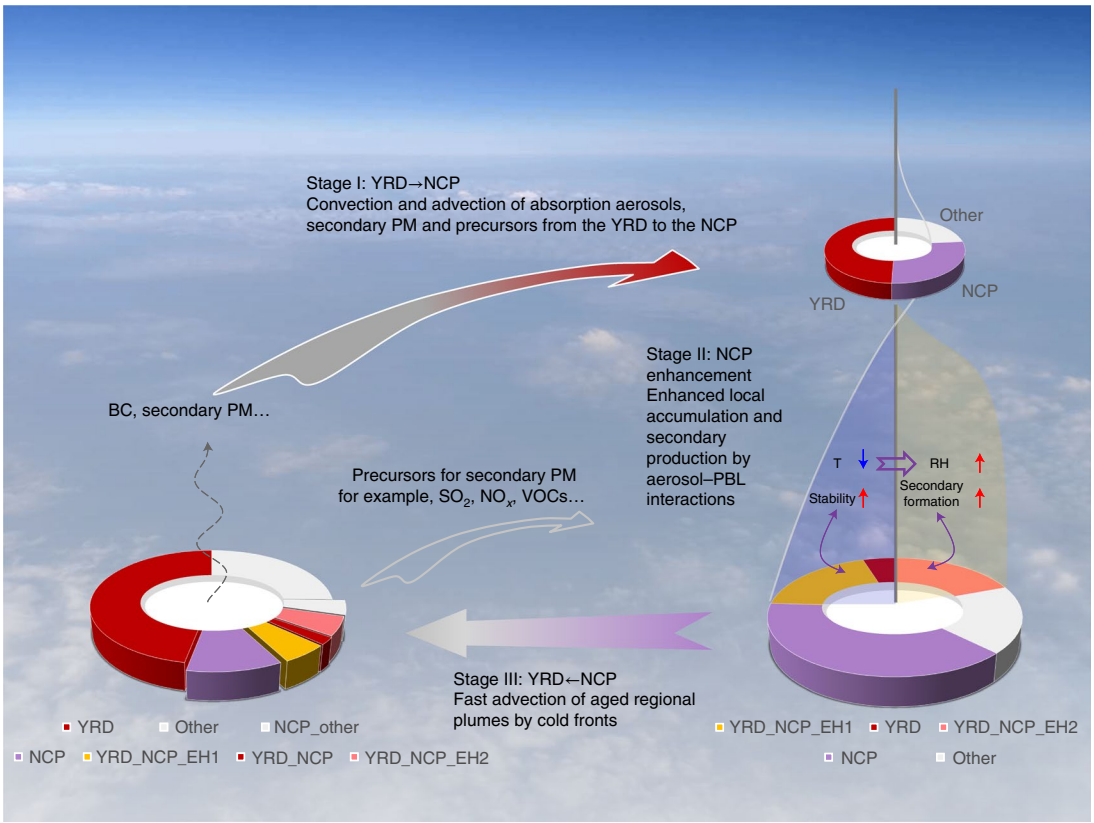


**Fig. 4 | A conceptual scheme of amplified transboundary transport of haze pollution by aerosol–PBL interactions.** Pie charts give the source apportionment of $PM_{2.5}$. The transparent blue and brown areas indicate the changes in air temperature and RH vertical profiles over the NCP. In the YRD pie chart, the quarter with the longer radius represents the impact of long-range transport from the NCP back to the YRD. YRD_NCP_EH1 and YRD_NCP_EH2 mean the enhancements of $PM_{2.5}$ in the NCP from local accumulation and secondary formation, respectively, amplified by aerosol–PBL interaction under the influence of upper-PBL regional sources from the YRD. YRD_NCP means contribution of aged YRD air masses recirculated back from NCP.

air temperature in the lower PBL leads to a substantial enhancement in RH, which favours aqueous-phase and heterogeneous chemical production of secondary aerosols. In the last stage, strong synoptic weather patterns, such as cold fronts, can then transport the enhanced primary and secondary PM back with precursors from both local and regional sources (Fig. 4 and Extended Data Fig. 7). The evolution of latitudinal distributions in WRF-Chem simulated $PM_{2.5}$ concentration and feedback-induced air temperature and RH changes during the three stages clearly show the amplified transboundary transport of haze pollution by aerosol–PBL interaction between the two regions (Fig. 5a-b).

WRF-Chem simulations for the other 17 events, identified in Supplementary Fig. 2, suggest that this conceptual scheme of enhanced haze events due to transboundary transport and aerosol–PBL interaction holds true more generally, beyond the December 2017 event. As shown in Extended Data Fig. 8 and Supplementary Fig. 5, all events feature a similar three-stage evolution as in Fig. 5a, and the aerosol–radiation interaction could cause substantial $PM_{2.5}$ enhancement in both the NCP region and the plumes transported back to the YRD (Supplementary Fig. 5). Although the patterns and magnitude may vary from case to case, the overall results display high similarity to the December 2017 event (Supplementary Fig. 6). The key roles of aerosol–PBL interaction on horizontal distribution and vertical structure are also clearly demonstrated by Extended Data Fig. 9.

Because the NCP and YRD are the two largest developed regions in China with great air quality concerns, the mechanism described here is expected to have very important implications for air pollution control policy making. Currently, besides overall improvement of technology-based emission reduction[40], strict short-term emission control actions are usually carried out for the early warning of severe haze on the basis of the air quality forecast[4,5,7,8]. Usually, such daily-based emission reduction takes action only after the predicted $PM_{2.5}$ concentration reaches a specific threshold. For the cross-year event in YRD, the early warning normally only started after 30 December (that is, when the regional plumes arrived). However, our model simulations show that a short-term emission cut in earlier days (for example, 26–27 December) when pollution was not that severe, could accomplish substantial pollution mitigation in the NCP and also benefit the YRD through a remarkable reduction of $PM_{2.5}$ peak, mainly secondary SNA, as the plumes transported back (Fig. 5c,d). For the in-advance emission reduction in the YRD, BC control is the most efficient means to mitigate the cross-regional haze pollution because of its critical role in the aerosol–PBL interaction on a regional scale (Supplementary Fig. 5). Such impacts of in-advance emission reduction on cross-region pollution mitigation are also well demonstrated by WRF-Chem simulations for other typical events in each year during 2013–2017 (Extended Data Fig. 10). Our results presented here clearly indicate the importance of understanding the complex feedback loop on a regional scale covering distances over 1,000 km and propose a unique solution for mitigating both local pollution and transboundary transport by a cross-regional coordinated effort based on more-accurate prediction of the onset of haze events.

## Online content

Any methods, additional references, Nature Research reporting summaries, source data, extended data, supplementary information,

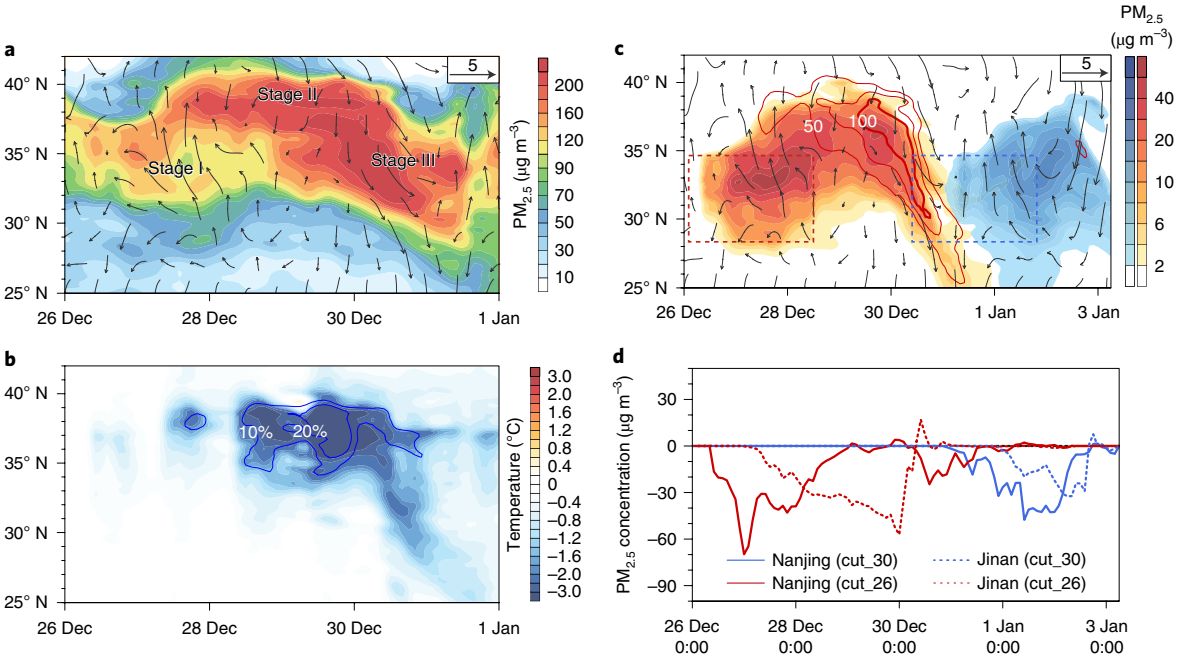


**Fig. 5 | Implications of aerosol–PBL interaction on cross-regional coordinated emission control. a**, Simulated evolution of zonal wind and $PM_{2.5}$ concentrations averaged over 115–120° E. **b**, Zonal averaged temperature and RH responses due to aerosol–PBL interaction derived from the difference between the runs with/without aerosol radiative effect. **c**, Zonal averaged SN concentration (red isolines) and $PM_{2.5}$ reduction due to 2 d 50% emission cut in YRD from 26 December (red shadow) and 30 December (blue shadow) 2017, respectively. **d**, Time series of $PM_{2.5}$ change at Nanjing and Jinan due to 2 d 50% emission cut in YRD from the two periods corresponding to **c**.

acknowledgements, peer review information; details of author contributions and competing interests; and statements of data and code availability are available at https://doi.org/10.1038/s41561-020-0583-4.

Received: 16 June 2019; Accepted: 28 April 2020;
Published online: 25 May 2020

## References

1. Huang, R. J. et al. High secondary aerosol contribution to particulate pollution during haze events in China. *Nature* **514**, 218–222 (2014).
2. Ding, A. J. et al. Enhanced haze pollution by black carbon in megacities in China. *Geophys. Res. Lett.* **43**, 2873–2879 (2016).
3. Guo, S. et al. Elucidating severe urban haze formation in China. *Proc. Natl Acad. Sci. USA* **111**, 17373–17378 (2014).
4. Li, H. et al. Rapid transition in winter aerosol composition in Beijing from 2014 to 2017: response to clean air actions. *Atmos. Chem. Phys.* **19**, 11485–11499 (2019).
5. Ding, A. et al. Significant reduction of $PM_{2.5}$ in eastern China due to regional-scale emission control: evidences from the SORPES station, 2011–2018. *Atmos. Chem. Phys.* **19**, 11791–11801 (2019).
6. Gao, M. et al. China's Clean Air Action has suppressed unfavorable influences of climate on wintertime $PM_{2.5}$ concentrations in Beijing since 2002. *Atmos. Chem. Phys.* **20**, 1497–1505 (2020).
7. Wang, J. D. et al. Particulate matter pollution over China and the effects of control policies. *Sci. Total Environ.* **584**, 426–447 (2017).
8. Sheehan, P., Cheng, E. J., English, A. & Sun, F. H. China's response to the air pollution shock. *Nat. Clim. Change* **4**, 306–309 (2014).
9. Huang, X., Wang, Z. L. & Ding, A. J. Impact of aerosol-PBL interaction on haze pollution: multiyear observational evidences in North China. *Geophys. Res. Lett.* **45**, 8596–8603 (2018).
10. Zhang, R. Y. et al. Formation of urban fine particulate matter. *Chem. Rev.* **115**, 3803–3855 (2015).
11. Zhang, Y. et al. Impact of synoptic weather patterns and inter-decadal climate variability on air quality in the North China Plain during 1980–2013. *Atmos. Environ.* **124**, 119–128 (2016).
12. Cai, W. J., Li, K., Liao, H., Wang, H. J. & Wu, L. X. Weather conditions conducive to Beijing severe haze more frequent under climate change. *Nat. Clim. Change* **7**, 257–262 (2017).
13. Callahan, C. W., Schnell, J. L. & Horton, D. E. Multi-index attribution of extreme winter air quality in Beijing, China. *J. Geophys. Res. Atmos.* **124**, 4567–4583 (2019).
14. Zhang, G. et al. Seesaw haze pollution in North China modulated by the sub-seasonal variability of atmospheric circulation. *Atmos. Chem. Phys.* **19**, 565–576 (2019).
15. Zhang, Q. et al. Transboundary health impacts of transported global air pollution and international trade. *Nature* **543**, 705–709 (2017).
16. Li, K., Liao, H., Cai, W. J. & Yang, Y. Attribution of anthropogenic influence on atmospheric patterns conducive to recent most severe haze over Eastern China. *Geophys. Res. Lett.* **45**, 2072–2081 (2018).
17. Ding, A. J. et al. Ozone and fine particle in the western Yangtze River Delta: an overview of 1 yr data at the SORPES station. *Atmos. Chem. Phys.* **13**, 5813–5830 (2013).
18. Cheng, Y. F. et al. Reactive nitrogen chemistry in aerosol water as a source of sulfate during haze events in China. *Sci. Adv.* **2**, e1601530 (2016).
19. Wang, G. H. et al. Persistent sulfate formation from London fog to Chinese haze. *Proc. Natl Acad. Sci. USA* **113**, 13630–13635 (2016).
20. Xie, Y. N. et al. Enhanced sulfate formation by nitrogen dioxide: implications from in situ observations at the SORPES station. *J. Geophys. Res. Atmos.* **120**, 12679–12694 (2015).
21. Zheng, G. J. et al. Exploring the severe winter haze in Beijing: the impact of synoptic weather, regional transport and heterogeneous reactions. *Atmos. Chem. Phys.* **15**, 2969–2983 (2015).
22. Sun, Y. L. et al. Investigation of the sources and evolution processes of severe haze pollution in Beijing in January 2013. *J. Geophys. Res. Atmos.* **119**, 4380–4398 (2014).
23. Moch, J. M. et al. Contribution of hydroxymethane sulfonate to ambient particulate matter: a potential explanation for high particulate sulfur during severe winter haze in Beijing. *Geophys. Res. Lett.* **45**, 11969–11979 (2018).
24. Ding, A. J. et al. Intense atmospheric pollution modifies weather: a case of mixed biomass burning with fossil fuel combustion pollution in eastern China. *Atmos. Chem. Phys.* **13**, 10545–10554 (2013).
25. Dong, Z. P. et al. Opposite long-term trends in aerosols between low and high altitudes: a testimony to the aerosol–PBL feedback. *Atmos. Chem. Phys.* **17**, 7997–8009 (2017).
26. Li, Z. Q. et al. Aerosol and boundary-layer interactions and impact on air quality. *Natl Sci. Rev.* **4**, 810–833 (2017).
27. Petäjä, T. et al. Enhanced air pollution via aerosol–boundary layer feedback in China. *Sci. Rep.* **6**, 18998 (2016).

28. Wang, Z., Huang, X. & Ding, A. Dome effect of black carbon and its key influencing factors: a one-dimensional modelling study. *Atmos. Chem. Phys.* **18**, 2821–2834 (2018).
29. Gao, M. et al. Modeling study of the 2010 regional haze event in the North China Plain. *Atmos. Chem. Phys.* **16**, 1673–1691 (2016).
30. Yang, Y. Q. et al. PLAM—a meteorological pollution index for air quality and its applications in fog–haze forecasts in North China. *Atmos. Chem. Phys.* **16**, 1353–1364 (2016).
31. Lou, S. J. et al. Black carbon amplifies haze over the North China Plain by weakening the East Asian winter monsoon. *Geophys. Res. Lett.* **46**, 452–460 (2019).
32. Ramanathan, V. et al. Warming trends in Asia amplified by brown cloud solar absorption. *Nature* **448**, 575–578 (2007).
33. Jacobson, M. Z. Strong radiative heating due to the mixing state of black carbon in atmospheric aerosols. *Nature* **409**, 695–697 (2001).
34. Cappa, C. D. et al. Radiative absorption enhancements due to the mixing state of atmospheric black carbon. *Science* **337**, 1078–1081 (2012).
35. Bond, T. C. et al. Bounding the role of black carbon in the climate system: a scientific assessment. *J. Geophys. Res. Atmos.* **118**, 5380–5552 (2013).
36. Nair, V. S., Babu, S. S., Manoj, M. R., Moorthy, K. K. & Chin, M. Direct radiative effects of aerosols over South Asia from observations and modeling. *Clim. Dynam.* **49**, 1411–1428 (2017).
37. Wilcox, E. M. et al. Black carbon solar absorption suppresses turbulence in the atmospheric boundary layer. *Proc. Natl Acad. Sci. USA* **113**, 11794–11799 (2016).
38. Bharali, C., Nair, V. S., Chutia, L. & Babu, S. S. Modeling of the effects of wintertime aerosols on boundary layer properties over the Indo Gangetic Plain. *J. Geophys. Res. Atmos.* **124**, 4141–4157 (2019).
39. Harris, E. et al. Enhanced role of transition metal ion catalysis during in-cloud oxidation of $SO_2$. *Science* **340**, 727–730 (2013).
40. Wang, C. Y., Li, P. G. & Liu, Y. Investigation of water-energy-emission nexus of air pollution control of the coal-fired power industry: a case study of Beijing-Tianjin-Hebei region, China. *Energy Policy* **115**, 291–301 (2018).

## Methods

**Observational data.** Ground-based observations of $PM_{2.5}$ concentrations at more than 1,500 stations since 2013 are archived at the air monitoring data centre of the Ministry of Ecology and Environment of China (available at http://datacenter.mep.gov.cn), which were collected to analyse spatiotemporal variations in eastern China. Since secondary aerosols, such as sulfate and nitrate, play a crucial role during haze pollution events in China, we also conducted in situ measurements of chemical compositions of ambient aerosols, such as sulfate, nitrate, ammonium, organic carbon and BC. In Nanjing, we routinely measured aerosols and their chemical compositions at the Stations for Observing Regional Processes of the Earth System. The instrumentation has been described in previous works[17,24]. During the winter season of 2017–2018, aerosol chemical compositions were also observed at the main cities in the NCP region, including Beijing, Tianjin, Shijiazhuang and Zhengzhou. The concentrations of sulfate, nitrate and ammonium were measured at these stations using the Monitor for Aerosols and Gases in Ambient Air. There was no direct observation on BC in Zhengzhou and Tianjin, and thus we used EC measurement by Sunset OC-EC instrumentation instead. At the Stations for Observing Regional Processes of the Earth System where both real-time BC and EC analysers were equipped, the variations of these two agreed quite well with each other but BC concentrations generally doubled those of EC (Supplementary Fig. 7). In addition to measurements on near-surface pollution, aerosol Lidar systems were operated in Shijiazhuang and Zhengzhou to provide vertical information on aerosol backscatters (relative concentrations of aerosols) and to better understand the patterns of pollution profile. To calculate synoptic variations, ensemble empirical mode decomposition was applied to decompose long-term observational data on $PM_{2.5}$ concentrations[41,42] into different intrinsic mode functions.

**Analysis of aerosol–PBL interaction.** In polluted regions such as eastern China, atmospheric aerosols can influence meteorological patterns by warming the upper air and blocking sunlight that would otherwise warm the Earth's surface. The opposite temperature responses to aerosols (atmospheric heating and surface dimming) make the air increasingly stable and stagnant. These effects then greatly inhibit the diffusion and dilution of pollutants, further worsening air quality levels through a phenomenon recognized as the aerosol–PBL feedback/interaction[2,9,28]. Comparisons of the air temperature stratification patterns observed from radiosonde observations and reanalysis data are usually used to manifest this effect[9]. In this work, GFS 24 h forecasts produced from a weather forecast model of the National Centers for Environmental Prediction (NCEP) are compared with radiosonde temperature and relative humidity observations to investigate the impacts of aerosol on atmospheric stratification and PBL meteorological patterns. The temperature and humidity profiles have been measured by radiosondes twice daily (0:00 and 12:00 UTC) from stations around the globe. Multiple stations, such as those in Beijing, Jinan, Zhengzhou and Nanjing, routinely conduct radiosonde observations. The mandatory pressure levels for measurements are 1,000, 925, 850 and 700 hPa for the lower troposphere[43]. The Integrated Global Radiosonde Archive compiles all radiosonde measurements into a quality-assured dataset.

**Identification of potential air mass source regions.** The Lagrangian particle dispersion model was used to identify transport pathways and to track potential sources of air masses during the studied pollution event using the Hybrid Single Particle Lagrangian Integrated Trajectory[44,45]. This model determines the positioning of particles from mean wind patterns and a turbulent transport component after they are released from a source point for forward simulations or from a receptor for backward runs as detailed in previous works[17,44,45]. In brief, 3,000 particles released every hour from a specific height and from the location of concern were then tracked forward or backward for three days in this work. Particle residence times of below 100 m were used to identify the 'footprint' retroplume, which can be interpreted as probability as potential source contribution for air masses released at the receptor[17,46]. The spatiotemporal distributions of these particles were used to identify potential source regions and their relative contributions to air masses at specific locations. During the haze episode, key cities located in the NCP and YRD regions or along the transport pathway included Tianjin, Zhengzhou and Nanjing. Therefore, the model calculations were performed for these cities when air pollution was locally accumulated or regionally transported.

**Regional coupled dynamical and chemical simulations.** To quantitatively understand the regional transport of pollution and corresponding roles of the aerosol–PBL interaction, coupled dynamic and chemical simulations were conducted on the basis of the WRF-Chem model (version 3.7.1). The WRF-Chem model is a state-of-the-art meteorology/chemistry model that considers a variety of coupled physical and chemical processes, such as the emission and deposition of pollutants, advection and diffusion, gaseous and aqueous chemical transformation, aerosol chemistry and dynamics, and so on[46]. The model has been widely used and evaluated against measurements and has been further improved by optimizing the parameterization of aqueous and heterogeneous chemistry in Asia[47,48].

In this work, we adopted two nested model domains. The parent domain with a grid resolution of 60 km covers eastern China and the surrounding areas. The spatial resolution of the inner domain is 20 km. There were 35 vertical layers from the ground level to the top pressure level of 50 hPa, in which more than 10 layers were settled under 1 km to better describe PBL processes. The simulation was conducted for the 18 typical cross-regional haze events during 2013–2018, including the 2017–2018 cross-year haze. In terms of the initial and boundary meteorological conditions, we used NCEP global final analysis data. NCEP Automated Data Processing surface and global upper air observational weather data for wind, temperature and moisture are assimilated to better characterize the regional transport patterns of air pollution. The Yonsei University PBL scheme was applied to parameterize PBL processes for this simulation. Other key parameterization tools include the Noah land surface scheme for describing land-atmosphere interactions, the Lin microphysics scheme with Grell cumulus parameterization for reproducing cloud and precipitation processes, and the RRTMG (Rapid Radiative Transfer Model for General Circulation Models) short- and long-wave radiation scheme. For the numerical representation of atmospheric chemistry, we use the Carbon-Bond Mechanism version Z photochemical mechanism combined with the Model for Simulating Aerosol Interactions and Chemistry aerosol module.

Both natural and anthropogenic emissions were considered for regional WRF-Chem modelling in the present work. Anthropogenic emissions generated via power plants, residential combustion, industrial processes, on-road mobile sources and agricultural activities were derived from the MIX Asian emission inventory database (Multi-resolution Emission Inventory for China)[49]. The Model of Emissions of Gases and Aerosols from Nature module embedded in the WRF-Chem model was used to calculate biogenic emissions online. This module estimates the net emission rates of isoprene, monoterpene and other biogenic volatile organic compounds from terrestrial ecosystems to the above-canopy atmosphere. Soil-derived dust emissions were characterized by Goddard Chemistry Aerosol Radiation and Transport emission schemes.

To determine the roles of aerosol–PBL interaction during the 18 typical cross-regional haze events during 2013–2018 (Supplementary Fig. 2), we conducted multiple parallel simulations using the WRF-Chem model. Our previous work has demonstrated that ARI has a strong influence on PBL meteorology under highly polluted conditions, especially when BC is present, given its strong capacity to efficiently absorb light[24,35,50]. Accordingly, two scenarios, one including and another excluding aerosols' radiative effects, were examined. The domain settings and model configurations used for these two simulations were exactly the same as those mentioned in the preceding. The simulations were initialized when the pollution levels had not yet deteriorated. No observational data were assimilated in these simulations. The model evaluation based on ground-based measurements in NCP and YRD cities suggests that the model simulations with ARI showed good performance (Supplementary Fig. 8). To identify the relative contributions from different regions, we also conducted multiple parallel runs (scenarios without anthropogenic emissions for one specific region). For example, contribution from YRD emissions can be quantified by comparing the scenario with all emission sources and that without YRD emissions. For the aforementioned simulations, the rate of the chemical species concentration change due to chemical production/loss processes is recorded at each time step to shed light on the chemical transformation from gas precursors to secondary aerosols. Thus, we derived the relative importance of different processes, including aerosol–PBL interaction and secondary transformation, on the basis of disparities between different simulation scenarios.

For the purpose of comparing the effectiveness of various emission control options, we also performed simulations with YRD emission cut by 50% for two days since 26 and 30 December and one scenario that cut only BC emission in the YRD. Similarly, simulation with 2 d in-advance emission reduction in the YRD was also conducted for other cases from 2013 to 2017 (Extended Data Fig. 10). To understand the role of aerosol–PBL interaction in temperature stratification during transport, the one-dimensional WRF-Chem single-column model was applied along the trajectory. Two simulation scenarios, ARI-on and ARI-off, were conducted. The model was initiated from Nanjing on 26 December with meteorological input from direct radiosonde observations. The aerosol concentrations extracted from the regional modelling results based on the trajectory locations were assimilated in the single-column model. The simulations were conducted over three days during which the air masses reached Beijing in the NCP region.

## Data availability

The observation and simulation data that support the main findings of this study are available at figshare data publisher (https://doi.org/10.6084/m9.figshare.9963311.v6). The emission input used in this work is the mosaic Asian anthropogenic emission inventory (MIX), which is archived at http://www.meicmodel.org/dataset-mix.html. The radiosonde measurements in Integrated Global Radiosonde Archive Version 2 are openly accessible at https://www1.ncdc.noaa.gov/pub/data/igra. The original simulation data for multiple cross-regional pollution events used in this study are stored in a high-performance computing centre of Nanjing University due to large data storage and can be made available from the corresponding author upon request.

## Code availability

Data processing techniques are available on request from the corresponding author. The source code of the WRF-Chem model is archived on UCAR data repository (http://www2.mmm.ucar.edu/wrf/users/download). The LPDM model can be acquired from the NOAA Air Resources Laboratory (ARL) for the provision of the HYSPLIT transport and dispersion model (http://www.ready.noaa.gov). The ensemble empirical mode decomposition (EEMD) analysis code that is embedded in NCAR Command Language version 6.40 is available at https://www.earthsystemgrid.org/dataset/ncl.640.html.

## References


41. Huang, N. E. et al. The empirical mode decomposition and the Hilbert spectrum for nonlinear and non-stationary time series analysis. *Proc. R. Soc. Lond. A* **454**, 903–995 (1998).
42. Wu, Z. & Huang, N. E. Ensemble empirical mode decomposition: a noise-assisted data analysis method. *Adv. Adapt. Data Anal.* **1**, 1–41 (2009).
43. Durre, I., Vose, R. S. & Wuertz, D. B. Overview of the Integrated Global Radiosonde Archive. *J. Clim.* **19**, 53–68 (2006).
44. Stein, A. F. et al. NAAA's HYSPLIT atmospheric transport and dispersion modeling system. *Bull. Am. Meteorol. Soc.* **96**, 2059–2077 (2015).
45. Ding, A. J., Wang, T. & Fu, C. B. Transport characteristics and origins of carbon monoxide and ozone in Hong Kong, South China. *J. Geophys. Res. Atmos.* **118**, 9475–9488 (2013).
46. Grell, G. A. et al. Fully coupled "online" chemistry within the WRF model. *Atmos. Environ.* **39**, 6957–6975 (2005).
47. Huang, X. et al. Direct radiative effect by multicomponent aerosol over China. *J. Clim.* **28**, 3472–3495 (2015).
48. Huang, X. et al. Pathways of sulfate enhancement by natural and anthropogenic mineral aerosols in China. *J. Geophys. Res. Atmos.* **119**, 14165–14179 (2014).
49. Li, M. et al. MIX: a mosaic Asian anthropogenic emission inventory under the international collaboration framework of the MICS-Asia and HTAP. *Atmos. Chem. Phys.* **17**, 935–963 (2017).
50. Huang, X. et al. Effects of aerosol–radiation interaction on precipitation during biomass-burning season in East China. *Atmos. Chem. Phys.* **16**, 1–37 (2016).


## Acknowledgements

This work was funded by the Ministry of Science and Technology of the People's Republic of China (2016YFC0200500), the National Natural Science Foundation of China (91544231, 41725020, 41922038 and 91744311), the National Research Program for Key Issues in Air Pollution Control in China (DQGG0107-03) and the Jiangsu Provincial Fund on $PM_{2.5}$ and $O_3$ pollution mitigation. We thank Q. Zhang and K. He at Tsinghua University for helpful suggestions and colleagues at Nanjing University and Environmental Monitoring Centers at Shijiazhuang, Zhengzhou, Tianjin and other cities in eastern and northern China for their contributions on the field measurements.

## Author contributions

A.D. and X.H. conceived the study and led the overall scientific questions. X.H., A.D., Z.W. and K.D. made the data analysis and modelling studies. J.G. and F.C. provided the measurement data for cities in northern China. X.H. and A.D. wrote the manuscript with contributions from all authors.

## Competing interests

The authors declare no competing interests.

## Additional information

**Extended data** is available for this paper at https://doi.org/10.1038/s41561-020-0583-4.

**Supplementary information** is available for this paper at https://doi.org/10.1038/s41561-020-0583-4.

**Correspondence and requests for materials** should be addressed to A.D.

**Peer review information** Primary Handling Editors: Xujia Jiang; Heike Langenberg; Rebecca Neely.

**Reprints and permissions information** is available at www.nature.com/reprints.

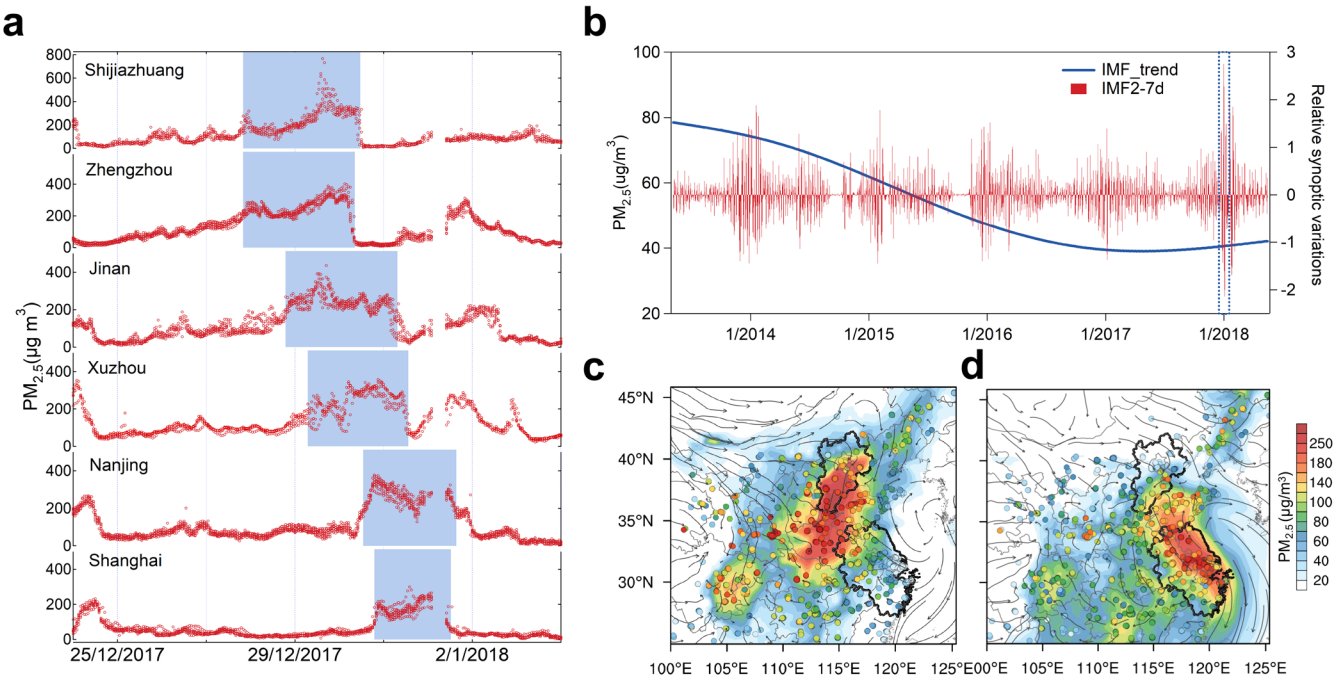


**Extended Data Fig. 1 | Time series and transport patterns of $PM_{2.5}$ in eastern China during the cross-year haze event. a**, $PM_{2.5}$ concentrations measured from Shijiazhuang, Zhengzhou, Jinan, Xuzhou, Nanjing and Shanghai in late December 2017 and early January 2018. Shaded squares mark the main periods of haze pollution for each city. **b**, Time series for low-frequency and relative synoptic variations (2-7 days) of $PM_{2.5}$ in Nanjing for 2013-2018. **c-d**, Average $PM_{2.5}$ concentrations and wind flows simulated by WRF-Chem for 28-29 December 2017 and 30 December 2017 – 1 January 2018, respectively.

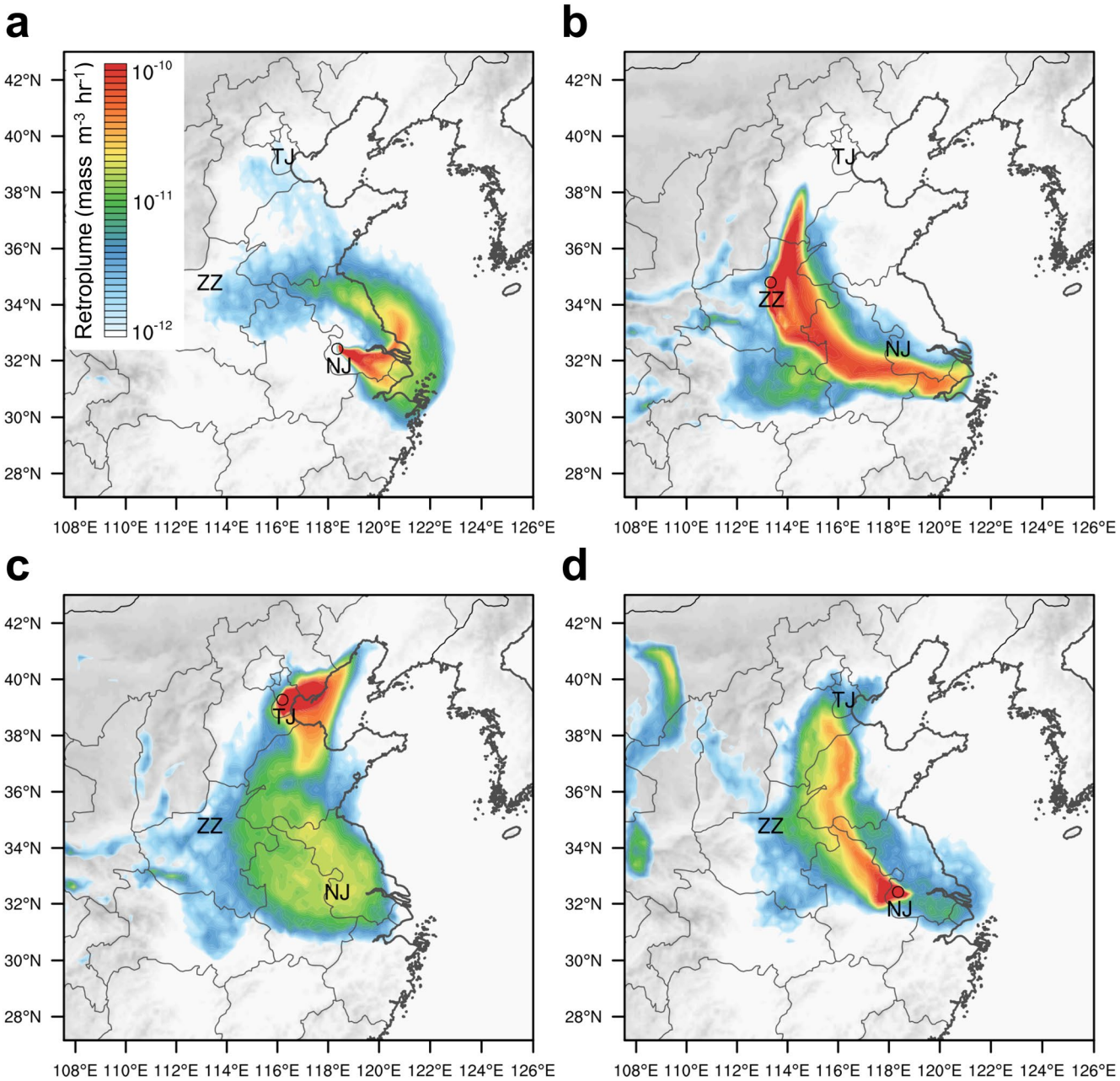


**Extended Data Fig. 2 | Regional transport characteristics during the cross-year haze event.** 72-hour retroplume ("footprint" residence time) showing transport pathways at Nanjing, Zhengzhou and Tianjin during this cross-region haze pollution. **a**, Nanjing (NJ) on 27 December; **b**, Zhengzhou (ZZ) on 28 December; **c**, Tianjin (TJ) on 29 December; **d**, Nanjing (NJ) on 31 December, 2017.

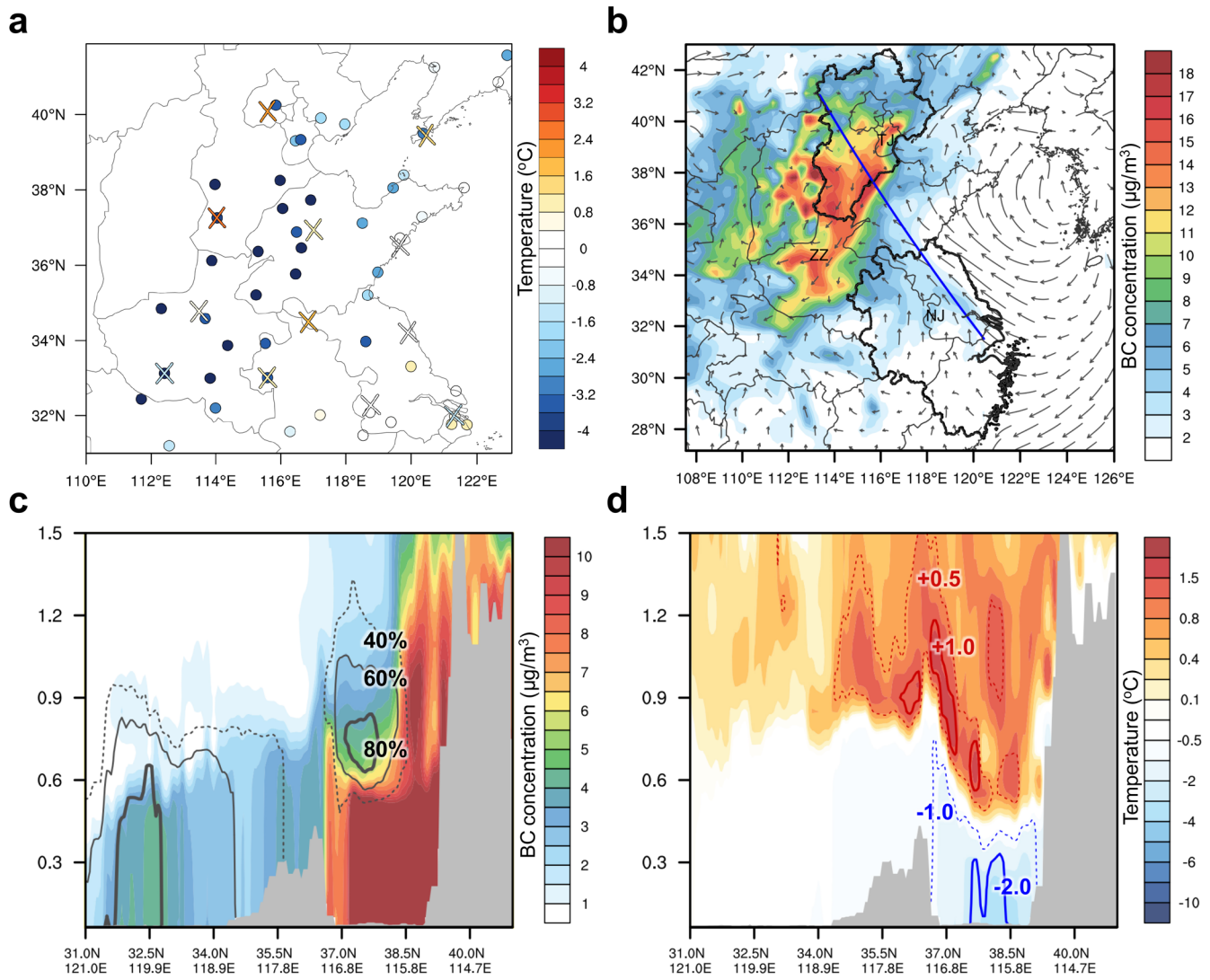


**Extended Data Fig. 3 | Evidence of intense aerosol-PBL feedback by regional transport between NCP and YRD. a**, Temperature difference between the 24-hour forecast by Global Forecast System (GFS) and radiosonde observations at 20:00 LT on 28 December, 2017. Note that circles mark the temperature disparities near the surface and crosses display those at 850 hPa. **b**, Spatial patterns of simulated BC concentration and wind at the same time with **a**. **c**, Cross section of vertical distribution of BC along the blue line in **b**. Grey lines denote the relative contribution from the YRD region. **d**, Cross section of simulated temperature difference due to aerosols' radiative effect (filled contour) and the relative contribution from YRD (isolines).

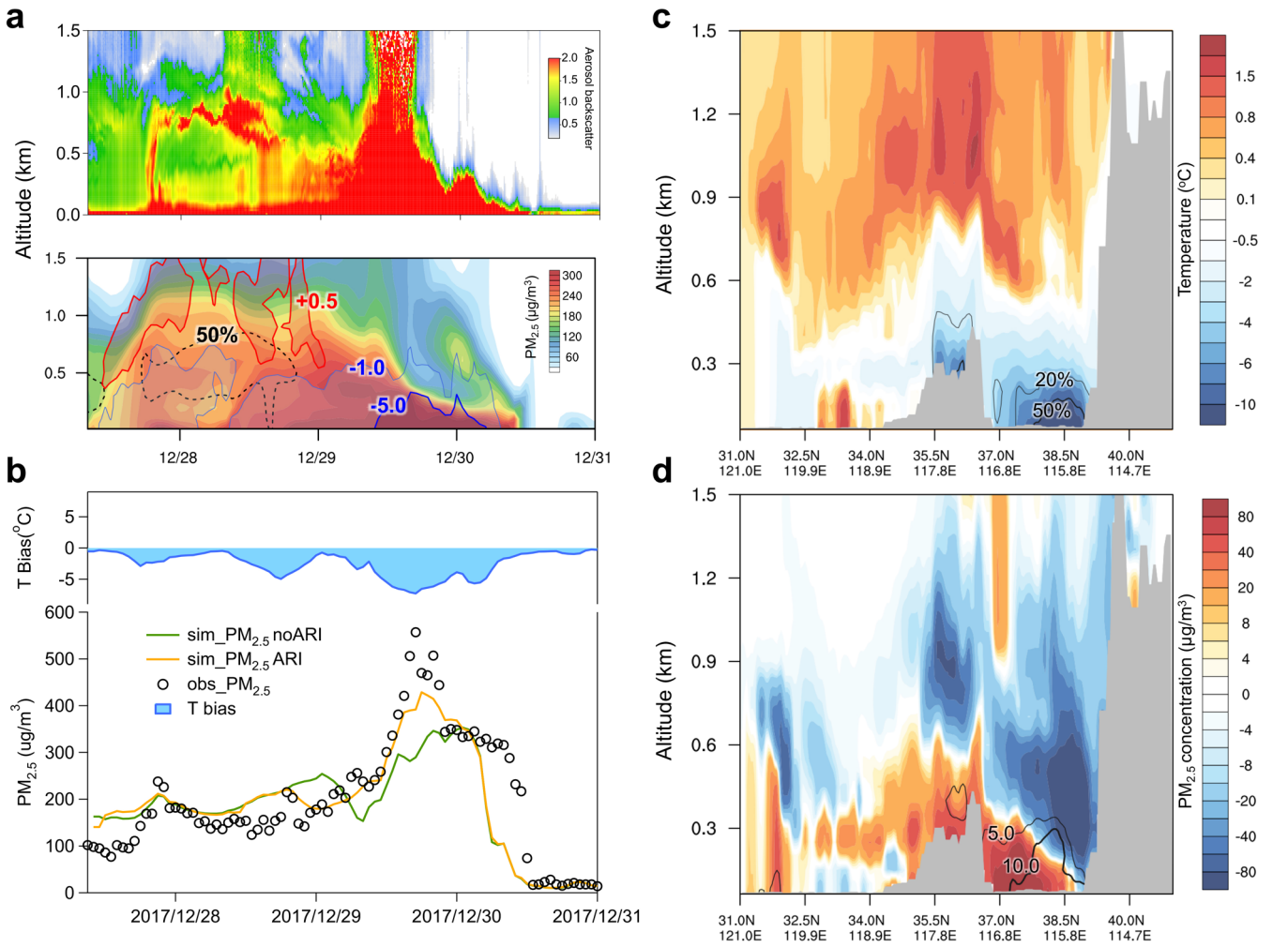


**Extended Data Fig. 4 | Vertical structure and evolution of aerosol-PBL feedback in North China. a**, Temporal variation of Lidar measured normalized aerosol backscatter and modeled $PM_{2.5}$ profiles at Shijiazhuang during 28-30 December 2017. Note that the dashed line marks the contribution from YRD emissions according to parallel simulations, and shadowed contour lines represent the temperature responses to ARI. **b**, Time series of difference between measured and simulated 2-meter air temperature without ARI, and time series of observed and simulated $PM_{2.5}$ concentrations with/without considering aerosols' radiative effect. **c**, Cross section of simulated difference in air temperature (filled contour) and relative humidity (isolines) due to ARI at 14:00 LT on 29 December, which was derived from the two simulation scenarios with and without ARI. **d**, Cross section of simulated difference in $PM_{2.5}$ concentration (filled contour) and secondary sulfate formation rate due to ARI.

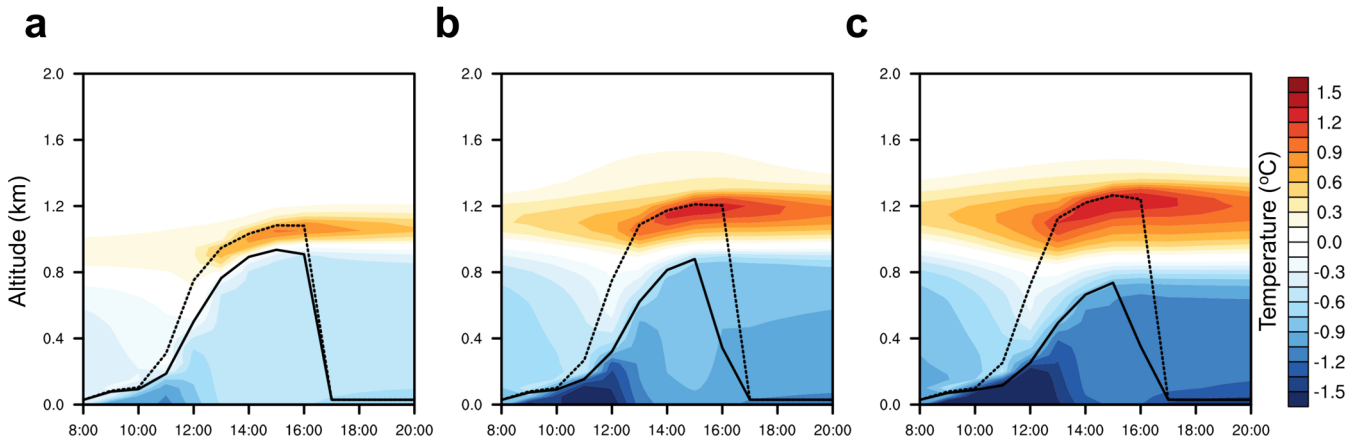


**Extended Data Fig. 5 | 1-Dimensional modeling of cumulative impact of aerosol-PBL feedback along the transport pathway of pollution. a-c**, Diurnal variation of vertical air temperature difference (contour) due to ARI at Nanjing on 26 December, Jinan on 27 December, and Beijing on 28 December, simulated by WRF-Chem SCM. Note that the solid and dashed lines mark the PBL height with/without considering ARI, respectively.

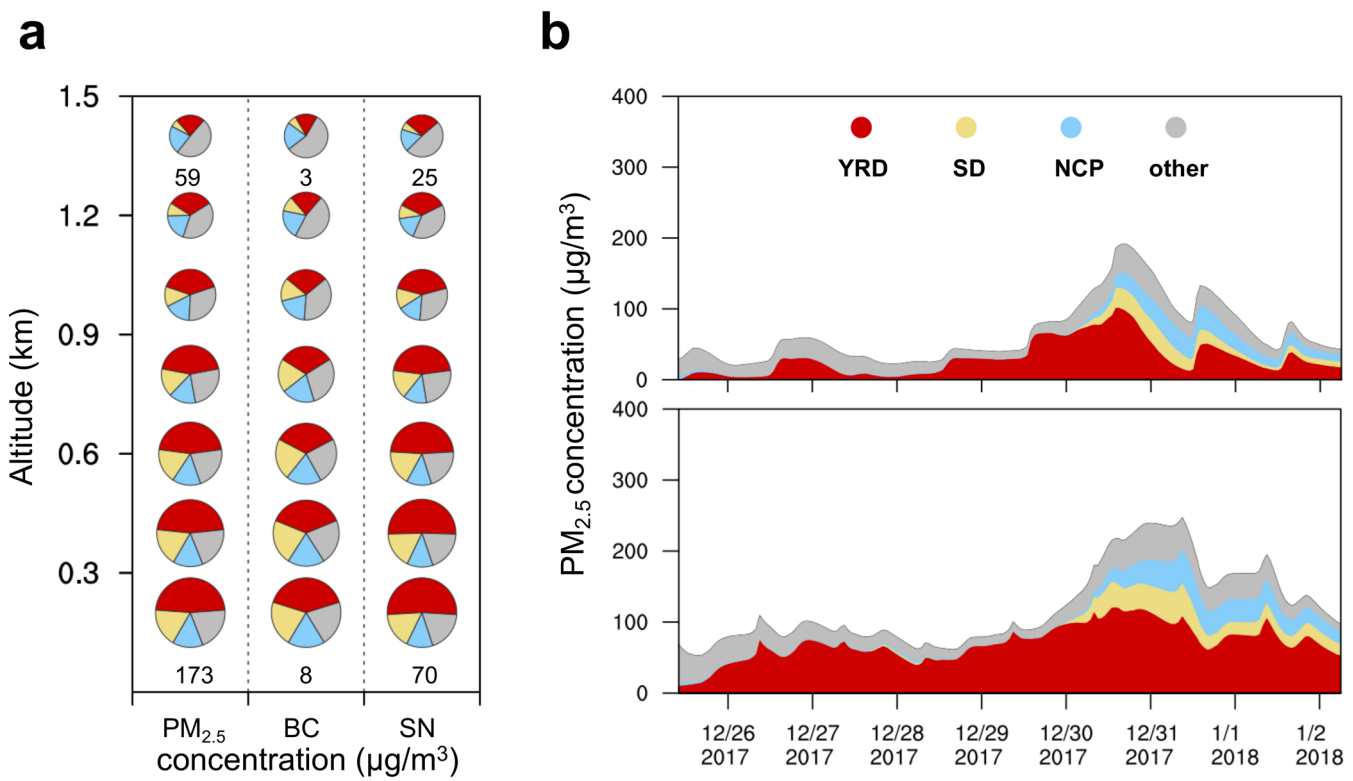


**Extended Data Fig. 6 | Enhanced haze pollution in YRD due to cross-regional transport. a**, Vertical distribution of the source appointment of $PM_{2.5}$, BC and SN (sulfate and nitrate) for YRD at different altitudes on 31 December derived from WRF-Chem simulations. The sizes of the pies denote the concentrations of $PM_{2.5}$, BC and SN, with numbers in a unit of μg $m^{-3}$ under the pies for reference. Red, yellow, blue and grey areas display contributions from YRD, Shandong (SD), NCP and other regions. **b**, WRF-Chem simulated $PM_{2.5}$ source appointment at the altitude of 700 m (upper panel) and at the ground surface (lower panel) of the YRD region.

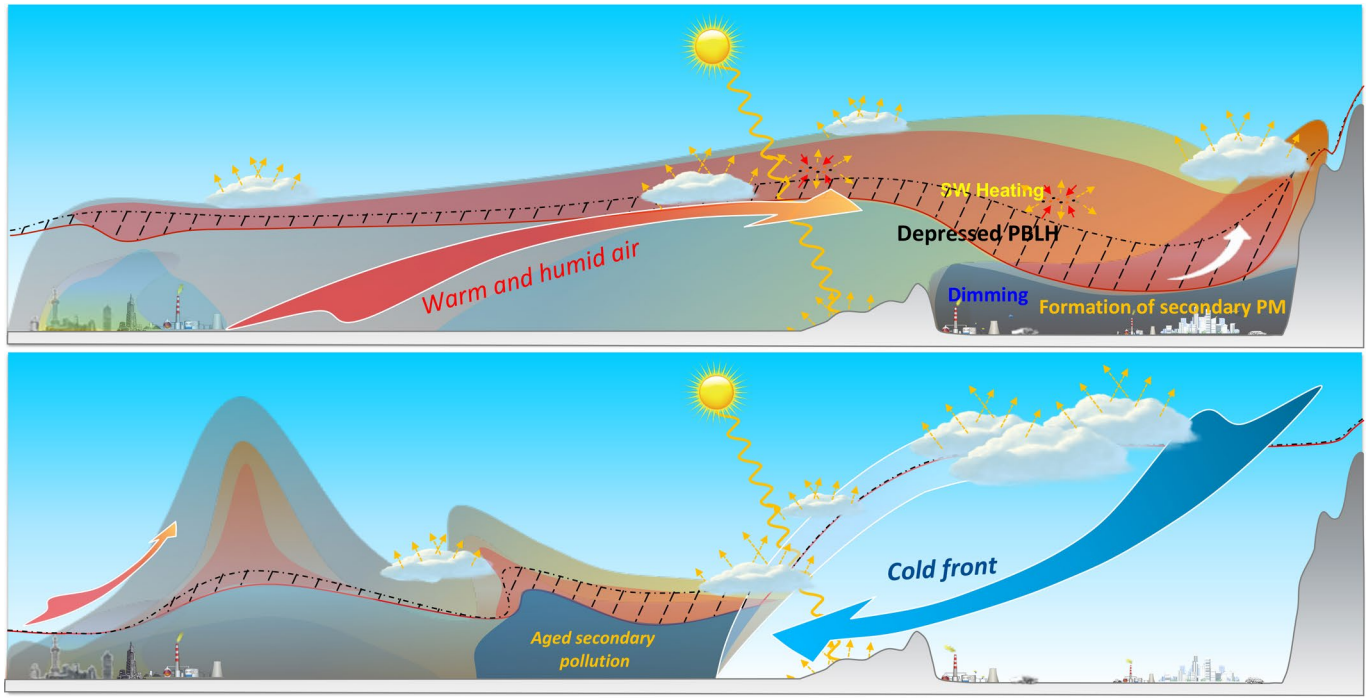


**Extended Data Fig. 7 | A conceptual scheme for the amplified transboundary transport of fine particles through aerosol-PBL feedback between YRD and NCP in China.** The upper panel shows how aerosol-PBL feedback was enhanced with depressed PBL, dimmed and humidified lower PBL when the warm and humid air transport from the YRD to NCP in the upper PBL. The lower panel shows how intensified aged secondary pollution in the NCP was transported to the YRD by cold fronts.

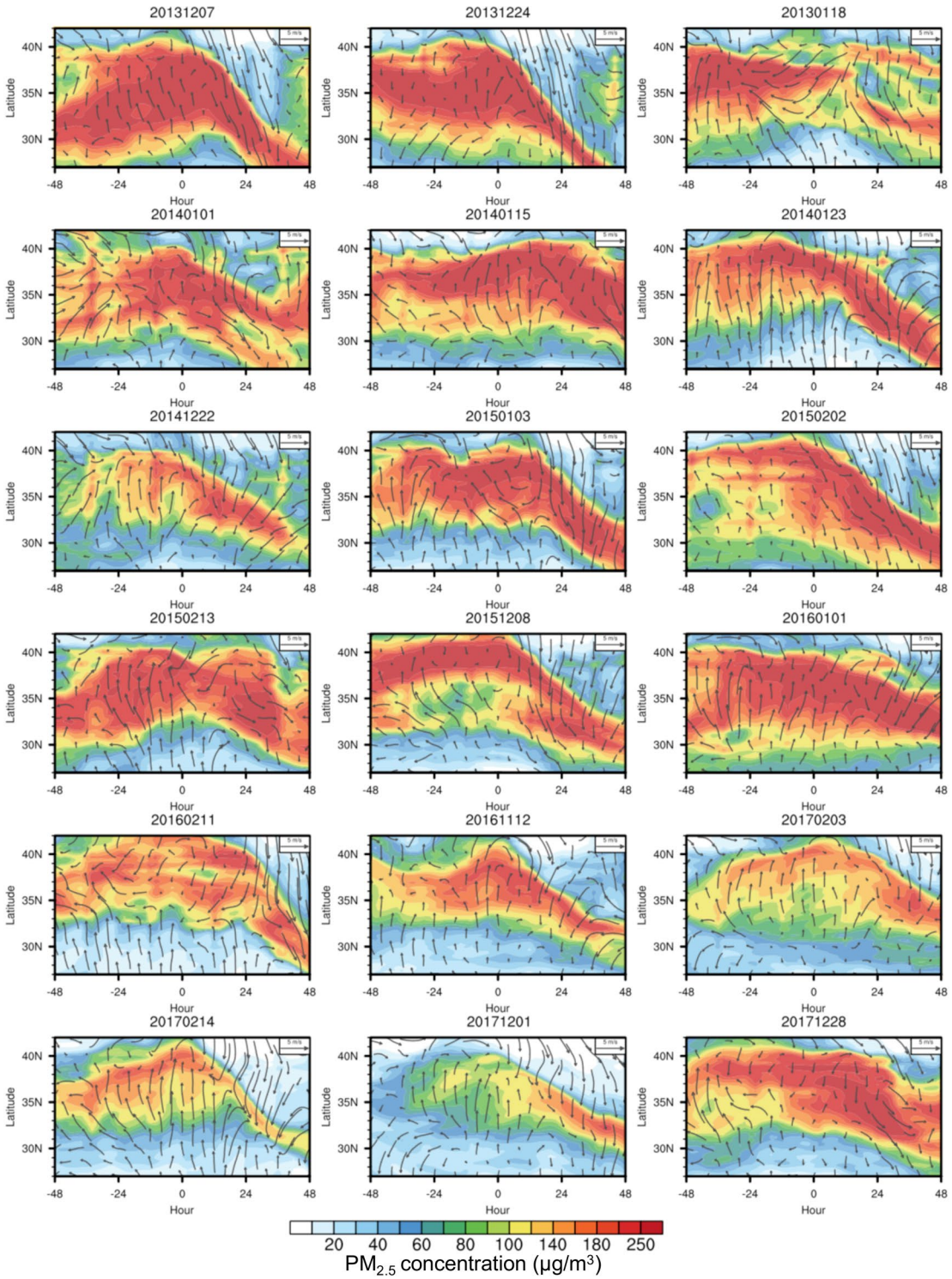


**Extended Data Fig. 8 | Evolution of transboundary transport of $PM_{2.5}$ for 18 pollution cases during 2013-2017.** WRF-Chem simulation of zonal averaged wind vector and $PM_{2.5}$ concentrations over 115-120 °E during 18 transboundary haze pollution cases. The time series of hourly $PM_{2.5}$ concentrations in NCP and YRD region in each case are presented in Supplementary Fig. 2. Note that the beginning date of each event is labelled above each subplot.

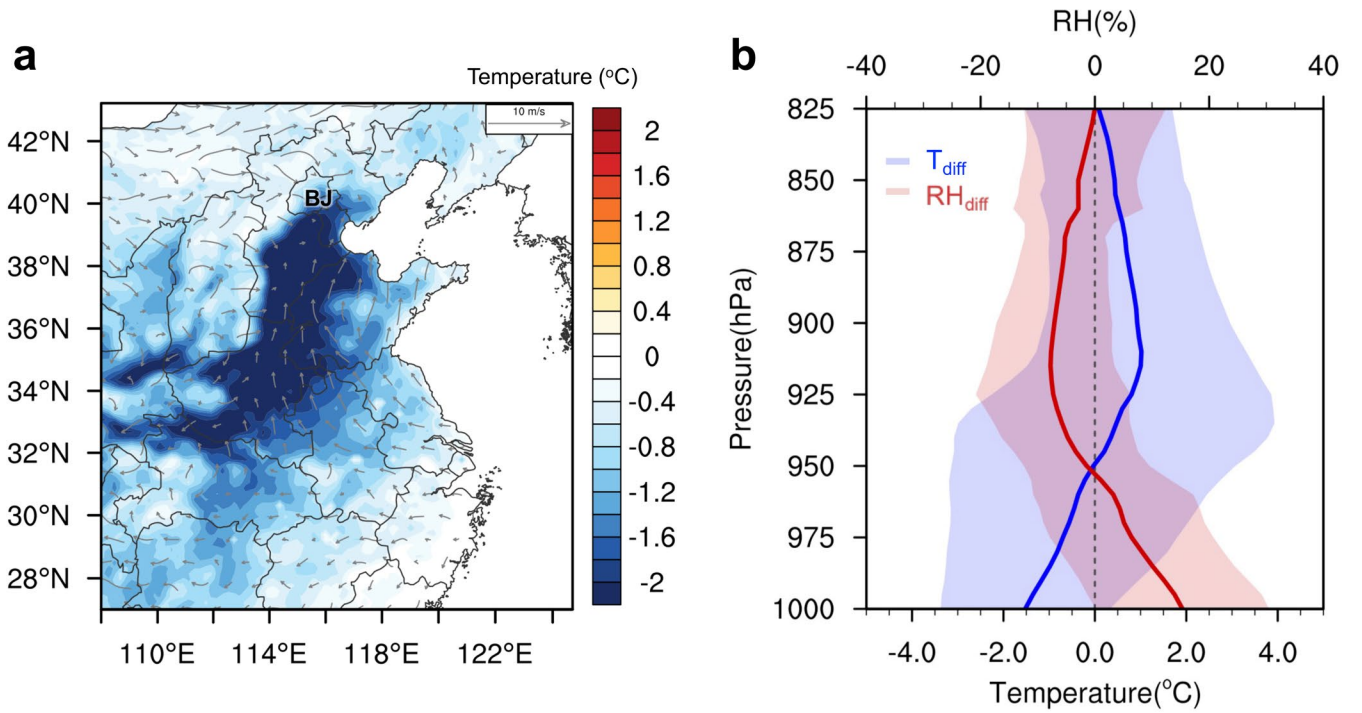


**Extended Data Fig. 9 | Air temperature response due to aerosol-PBL interaction. a**, averaged spatial distribution of 2-meter temperature responses to aerosol-PBL interaction and mean wind vectors during Stage II of 18 cross-regional pollution events identified in Supplementary Fig. 2. **b**, Statistics of vertical profile of air temperature difference ($T_{diff}$) and RH difference ($RH_{diff}$) between radiosonde observations and GFS 24-hour forecast at Beijing when haze pollution peaked in NCP. Lines and shaded areas mark the average and standard deviations, respectively.

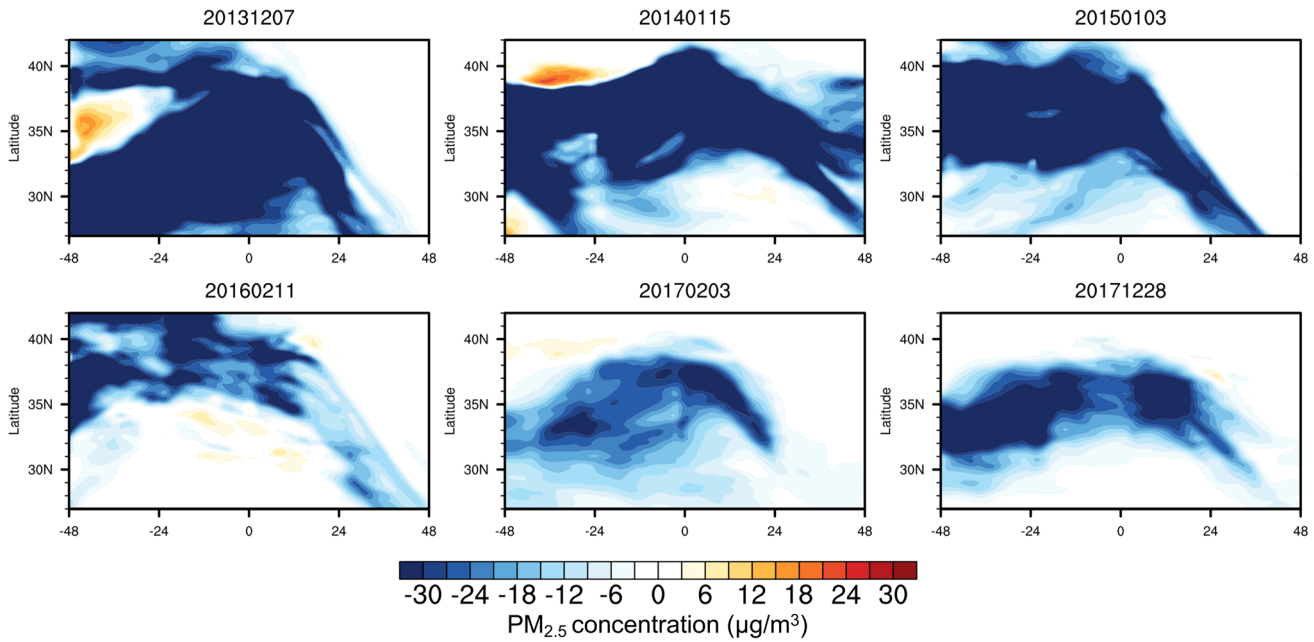


**Extended Data Fig. 10 | Regional-scale $PM_{2.5}$ mitigation due to in-advance and cross-regional coordinated emission control.** Zonal averaged $PM_{2.5}$ reduction over 115-120 °E due to 2-day 50% emission cut in YRD before Stage I for 6 typical cross-regional cases during 2013-2017. Note that the beginning date of each event is labelled above each subplot.